Proceedings 10th NUMGE 2023
10th European Conference on Numerical Methods in Geotechnical Engineering
Zdravkovic L, Kontoe S, Taborda DMG, Tsiampousi A (eds)

https://doi.org/10.53243/NUMGE2023-41

Investigation of numerical modelling approaches for diaphragm walls with support of inverse parameter identification

H. Jürgens[1], S. Henke[1]

[1]*Department of Geotechnics, Helmut Schmidt University / University of the Federal Armed Forces, Hamburg, Germany*

ABSTRACT: Numerical investigations using Finite Element Analyses (FEA) with different modelling approaches for diaphragm walls are conducted considering a 20 m deep excavation pit with available horizontal deformation measurement data. The subsoil mainly consists of different sand layers. For realistic soil-behaviour representation, a high-quality constitutive model (Hardening Soil small strain stiffness) is used. The stiffness parameters are determined using inverse parameter identification (particle swarm optimization) by comparison with measured horizontal deformations of the wall. The measurement data show that the diaphragm wall has deflected significantly; therefore, a calibration with complete agreement with the classic linear-elastic wall consideration is not possible.
Based on this, the following approaches of modelling the diaphragm wall are investigated: linear-elastic continuum as well as structural elements, elastoplastic structural elements with a user-defined M-κ diagram and an elastoplastic concrete model. To identify the optimal modelling variant for a near-realistic representation of the soil-structure interaction, the bending moment distributions are compared. The results show that the excavation process causes plastic deformations of the wall, leading to higher horizontal deformations in the final state when the elastoplastic material models are considered.

Keywords: FEA; material models, excavation, PSO

1 INTRODUCTION

Diaphragm walls are widely used for the design of deep excavation pits in urban areas to prevent large deformations. In this paper, a nearly 20 m deep excavation pit in the city centre of Berlin is investigated. The surrounded soil predominantly consists of sand, thus necessitating a water-impermeable construction method. Therefore, in addition to the diaphragm wall, a jet grout slab is used at the bottom of the excavation to protect against pressurised water from below.

Considering the numerous interactions between different structural elements in the design of such deep excavations, conventional methods can only be used by applying many assumptions. A Finite Element Analysis (FEA) is therefore recommended for such structures. FEA has been increasingly used in geotechnical engineering in recent decades and has become a common tool for analysing for example deformations, stresses and structural forces.

Compared to the conventional methods, the FEA offers several advantages. One of these is the use of complex constitutive models for the realistic simulation of soil-structure interaction. In this paper, different variants of concrete material models are investigated with the aim to model and design the diaphragm wall excavation pit more accurately. One variant is the use of the concrete constitutive model, which is described in detail in Schädlich and Schweiger (2014). Compared to the linear-elastic, perfectly plastic Mohr-Coulomb model, which is often used for modelling cementitious materials, the concrete model used can simulate softening in tension and compression (Schädlich and Borchert, 2017). Another variant discussed in this paper is the use of structural elements with elastoplastic behaviour in terms of an M-κ diagram. Based on this, the nonlinear moment curvature is determined to simulate the bending behaviour of reinforced concrete.

Furthermore, measurement data of the horizontal deformations from inclinometer readings are available for the investigated excavation pit. Based on this, the parameters for the advanced constitutive soil model Hardening Soil model with small strain stiffness (HSsmall) are determined using inverse parameter identification. Therefore, the Particle Swarm Optimization (PSO) algorithm stated by Kennedy and Eberhart (1995) is used. In Hajihassani et al. (2018) an overview of several geotechnical application cases using PSO is given. Especially Meier et al. (2009) employed the optimization strategy for the inverse parameter calculation on the basis of inclinometer readings. In this paper, PSO is used to adjust the

stiffness parameters of the sandy soils so that the calculated horizontal deformations match the readings measured from the inclinometer.

Based on the inverse parameter identification, the numerical model of the excavation pit is simulated using different material models (e.g. concrete model or M-κ diagram) for the diaphragm wall. Subsequently, the results are compared in terms of horizontal wall deformation as well as the bending moment distribution. In conclusion, a prediction should be made as to which material model is the most accurate for the simulation of the investigated diaphragm wall supported excavation pit in Berlin.

2 NUMERICAL MODEL OF THE EXCAVATION PIT

The investigated excavation pit (see Figure 1) is located in Berlin and has an 80 cm wide diaphragm wall, which is supported by two struts and one grout anchor. Directly behind, at the top of the wall, is a soldier pile wall. The ground level is dedicated at +36.2 m NHN. Due to unrealistically large base point rotation of the soldier pile wall towards the excavation pit and thus a missing supporting effect of the wall in first numericalsimulations, the area between the top of the diaphragm wall (+33.5 m NHN) and the ground level (+36.2 m NHN) is replaced by an equivalent vertical line load (g_k = 45.9 kN/m²) and a horizontal point load (G_k = 60.0 kN/m).

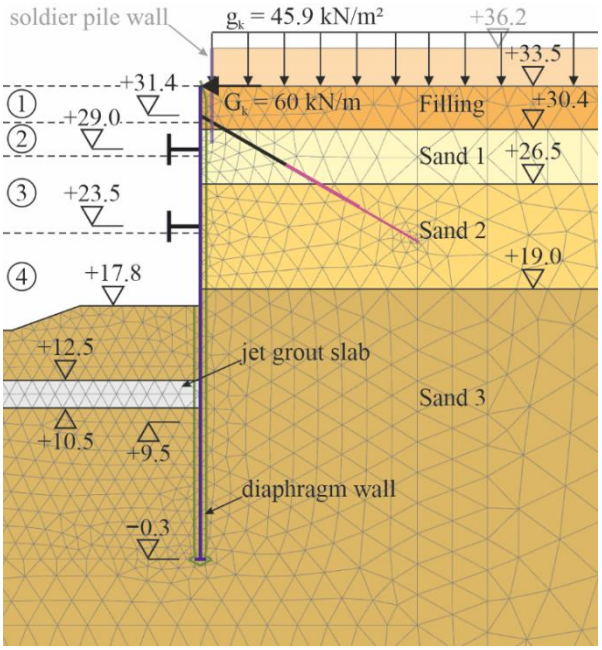

Figure 1. Numerical model and discretisation of the investigated excavation pit

The surrounded soil consists of a filling layer at the top and three different types of sand layers underneath. The groundwater head lies at +31.2 m NHN. Due to the water permeability of the sand and the deep excavation, a jet grout slab is used to vertically seal the pit. Simulating the jet grout slab material behaviour, the concrete material model with parameters stated by Schweiger et al. (2014) is used. Furthermore, the bottom edge of the diaphragm wall is extended from +9.5 m NHN to -0.3 m NHN due to the high water pressure difference in the final excavation state. Since then, the reinforced section of the wall has a length of 24 m (from +33.5 m NHN to 9.5 m NHN) and the unreinforced section is 9.8 m long.

The grout anchor is modelled by means of a node-to-node anchor for the unbounded length and an embedded beam row element considering a linear-elastic material model for the grout body. The anchor is prestressed with $F_{prestress} = 420\,kN$. Additionally, the maximum axial skin resistance τ_{skin} is calculated using the failure criterion after Mohr-Coulomb (see Equations 1-4), where σ_n is the effective normal stress and R_{inter} the interface strength factor specified in the interface element of the embedded beam row element.

$$\tau_{skin} = \sigma_n \cdot \tan \varphi_i' + c_i \quad (1)$$

$$\varphi_i' = R_{inter} \cdot \varphi_{soil} \quad (2)$$

$$c_i = R_{inter} \cdot c_{soil} \quad (3)$$

$$R_{inter} = \tan \delta / \tan \varphi_{soil} \quad (4)$$

3 INVERSE PARAMETER IDENTIFICATION

No laboratory tests are available to determine the soil parameters for the presented excavation pit. Therefore, inverse parameter identification is performed to identify a set of parameters that fits the measured horizontal deformation of the diaphragm wall with good agreement. A population-based stochastic optimization algorithm (Particle Swarm Optimization – PSO) is used with a defined number of point-shaped, collision-free particles n searching for a set of N_p unknown parameters. The problem is solved by minimising the objective function $\epsilon(z)$ (see Equation 5) in the N_p-dimensional search area. According to Levasseur et al. (2008), the least squares method is proposed as an objective function, which defines the differences between measured and calculated horizontal deformation summed up over the wall length.

$$\epsilon(z) = \sqrt{\frac{1}{N}\sum_{i=1}^{N}\left(\frac{u_{x,i,meas}(z) - u_{x,i,calc}(z)}{u_{x,i,meas}(z)}\right)^2} \quad (5)$$

Here, N is the number of measurement points, $u_{x,i,meas}$ is the i^{th} measured horizontal deformation and $u_{x,i,calc}$ is the i^{th} calculated horizontal deformation.

The inclinometer in the diaphragm wall has a length of 24 m from the top of the wall (+33.5 m) to the end of the reinforced section (+9.5 m) with a measurement point every half metre. For the inverse parameter calibration, the diaphragm wall is modelled by means of a linear-elastic structural element as it is typically used in FEA considering diaphragm walls.

The PSO is defined with $n = 10$ particles and a maximum number of iterations $\max iter = 50$. The inertia, cognitive and social coefficients are set to: $c_1 = c_2 = 2$ following the proposal of Kennedy and Eberhart (1995) and $\omega = 1$ to facilitates an exploration in the entire search space.

In the numerical simulation, the Hardening Soil Small model is employed for the three sand layers, considering hardening plasticity and small strain stiffness according to Schanz et al. (1999) and Benz (2007). The filling is modelled using a linear-elastic model including the failure criterion after Mohr-Coulomb. For the PSO, only the stiffness parameter from drained triaxial tests E_{50}^{ref} and the stiffness parameter m, respectively, the oedometric stiffness E_{oed} for the filling are varied. The remaining stiffness parameters for the Hardening Soil Small model are calculated by means of the following correlations: $E_{50}^{ref} = E_{oed}^{ref} = 3 \cdot E_{ur}^{ref}$. For the small strain parameters, an assumption following op de Kelder (2015) is used. Table 1 shows the soil parameters as a result of the PSO.

Table 1. Material parameters for the soils investigated: HSS-model for sand and MC-model for filling

Parameters		Filling	Sand 1	Sand 2	Sand 3
γ	[kN/m³]	17	17.5	18	18.5
γ_{sat}	[kN/m³]	20	20	20.5	20.5
φ'	[°]	30	32.5	35	37.5
c'	[kN/m²]	0	0	0	0
ψ	[°]	0	2.5	5	7.5
E_{oed}	[MN/m²]	28.7	-	-	-
ν	[-]	0.3	-	-	-
E_{50}^{ref}	[MN/m²]	-	37.94	60.30	80.40
E_{oed}^{ref}	[MN/m²]	-	37.94	60.30	80.40
E_{ur}^{ref}	[MN/m²]	-	113.82	180.91	214.19
m	[-]	-	0.496	0.469	0.491
p_{ref}	[kN/m²]	-	100	100	100
G_0	[MN/m²]	-	294.58	387.14	485.71
$\gamma_{0.7}$	[-]	-	$5 \cdot 10^{-5}$	$3.8 \cdot 10^{-5}$	$3.3 \cdot 10^{-5}$

Furthermore, Figure 2 shows the measured $u_{x,i,meas}(z)$ and the calculated horizontal deformation $u_{x,i,calc}(z)$ from the PSO with respect to depth z. The fixed point of the inclinometer is assumed to be at the bottom end, which is why the horizontal displacement at this depth is $u_{x,i,meas}(z = 9.5\ \text{m}) = 0$. Therefore, the calculation results are adjusted so that measured and calculated data are the same at that point $u_{\text{x,i,meas}}(z = 9.5\ \text{m}) = u_{\text{x,i,calc}}(z = 9.5\ \text{m}) = 0$.

The results show that for the investigated excavation pit, the PSO is incapable to find a parameter set for which the calculated and measured horizontal deformations are in reasonable agreement. Note that in this investigation only the stiffness parameters are varied to avoid a change of the critical state line in the constitutive model. Since no laboratory tests are carried out to determine, for example, strength parameters, it is theoretically possible to optimize further parameters (e.g. friction angle φ' and cohesion c'). In the present study, this is considered not to be expedient due to an increased computational effort and only minor improvements. Additionally, the constitutive behaviour of the sand in Berlin is very well known, hence HSsmall parameters with similar strength parameters have already been determined at other locations. A deviation from these should therefore only occur on a small scale.

It is evident to note, that this is an example of an excavation pit with unexpectedly high deformations. The reasons for the high values of measured deformations are complex and remained unclear. One reason can be settlements caused by surrounding construction works. The excavation pit is located directly in the area of the Alexanderplatz in Berlin, where several different projects are currently being realised. Therefore, it cannot be excluded that one of the surrounding projects influences the investigated excavation pit, but as no evidence of such influences can be found, this is considered not to be plausible. Another point is the inclinometer itself, which can provide erroneous readings, although this is not assumed as the instrument has been thoroughly checked. Therefore, further research is needed to determine the reasons for the discrepancy between measured and simulated deformations.

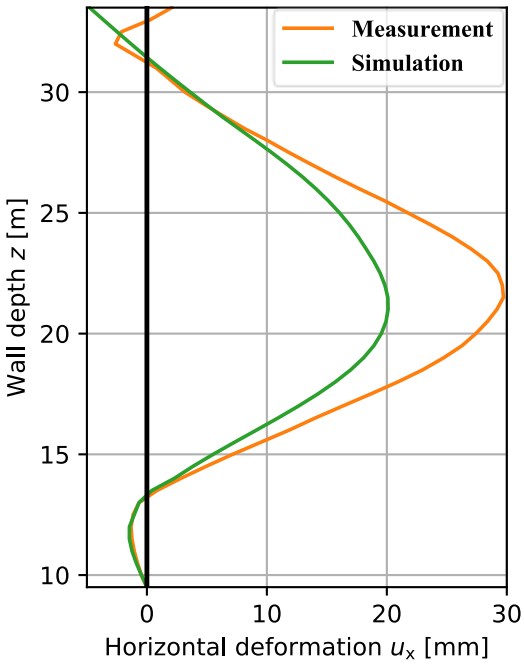

Figure 2. Measured and simulated horizontal deformations u_x of the diaphragm wall plotted over the wall depth z

The aim of this paper is to compare different approaches for modelling the diaphragm wall, considering linear-elastic versus elastoplastic material behaviour. As a starting point for this investigation the parameter set given in Table 1 is used.

4 MATERIAL MODELS FOR THE DIAPHRAGM WALL

The diaphragm wall is modelled considering four different approaches: linear-elastic continuum element (CE) (a) as well as structural element (SE) (b), elastoplastic SE with a user-defined M-κ diagram (c) and a CE with the elastoplastic concrete model (d). Figure 3 shows the different modelling variants in the numerical simulation.

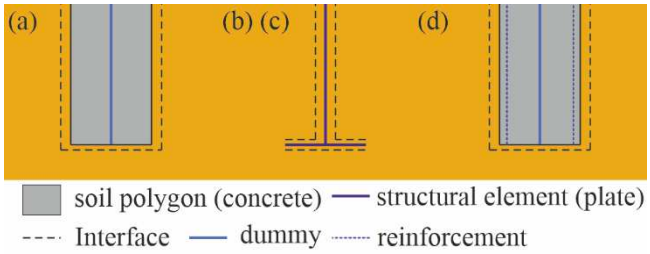

Figure 3. Variants of the investigated approaches for modelling the diaphragm wall at the base: linear-elastic CE (a), linear-elastic SE (b), elastoplastic SE with a user-defined M-κ diagram (c) and elastoplastic CE with concrete model (d)

A preliminary analysis using the limit equilibrium method indicated a reinforcement ratio of $A_{s,req} = 49.1\ \mathrm{cm^2/m}$ on both sides of the wall. The concrete to be used is C 30/37 with a reduced stiffness and strength of 80 % due to inaccuracies during construction. The wall friction coefficient is assumed to be $R_{inter} = 0.5$ for a wall frichtion angle of approx. $\delta = 1/2\varphi$.

Simulating the wall with a linear-elastic material model (a and b), only Young's modulus E and Poisson's ratio ν are required. In case of using a CE (a and d), a so-called dummy element is modelled in the centre of the cross-section, which contains material parameters reduced by a factor of 10^{-3}. For the CE with linear-elastic material model (a), the dummy element evaluates the internal forces and displacements of the diaphragm wall. However, when using CE with the elastoplastic concrete model (d), due to the changing stiffness during the plastification of the concrete, only the displacements of the wall are analysed using the dummy element and the internal forces are determined using the „*structural forces in volume plates*" feature of PLAXIS.

Regarding the diaphragm wall modelled using a SE (b and c), horizontal elements are provided at the wall's base representing the contact area for vertical load transfer.

In terms of simulating the wall with the elastoplastic material model (c), the wall is modelled by means of an SE with elastoplastic M-κ behaviour. Therefore, the bending stiffness EI and the axial stiffness EA are required. The required rate of steel $A_{s,req}$ is chosen as cross section A. Based on this, the moment of inertia I is adjusted so that the ratio of reinforcement to cross-section corresponds to the thickness of the structural element. The M-κ diagram is calculated based on the stress-strain curve for a reduced C30/37 (80%) from EC 2 (Figure 4).

The parameters for the elastoplastic concrete model (d) are given in Table 2 and are calibrated on the basis of the stress-strain curve for a reduced C30/37 (80%). Figure 4 shows a comparison of the theoretical stress-strain curve from EC 2 and the one simulated with PLAXIS SoilTest. Further parameters are selected based on the recommendations in the PLAXIS manual. Time effects of the material model are not considered in the numerical simulation. The reinforcement is simulated by defining additional structural elements with elastoplastic material behaviour. Therefore, the maximum bending moment and axial force are calculated based on the required amount of steel and the characteristic yield strength ($f_{y,char} = 500\ \mathrm{N/mm^2}$).

Figure 5 displays the calculated and measured horizontal deformations u_x along the diaphragm wall for all four investigated approaches. The results show that the simulation with linear-elastic CE almost shows the same deformations as the simulation output using the linear-elastic SE. In the case of using an elastoplastic material model (CE concrete model and SE M-κ), the calculated horizontal deformations are significantly higher compared to the simulations considering a linear-elastic material model. Plastic deformations that occur during construction and due to the installation of the supports obviously significantly influence the horizontal wall deformations in the final state of this complex excavation pit. Additionally, the horizontal deformations obtained from the simulation with elastoplastic wall behaviour are closer to the measured data.

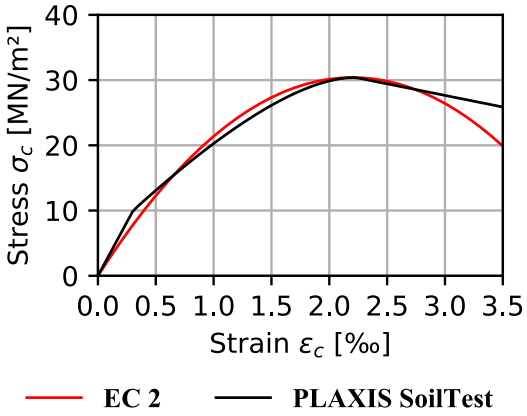

Figure 4. Stress-strain curve in compression for C30/37 with reduced strength and stiffness (80%)

Table 2. Material parameters for the concrete model

Parameters		Diaphragm wall (C30/37 – 80%)
E_{28}	[kN/m²]	26,400,000
ν	[-]	0.2
$f_{c,28}$	[kN/m²]	30,400
$f_{t,28}$	[kN/m²]	2,000
φ_{max}	[°]	35
f_{c0n}	[-]	0.33
f_{cfn}	[-]	0.85
f_{cun}	[-]	0.10
ε_{cp}^{p}	[-]	-0.0013
$G_{c,28}$	[kN/m]	40
f_{tun}	[-]	0
$G_{t,28}$	[kN/m]	0.05016
γ_{fc}	[-]	1.0
γ_{ft}	[-]	1.0

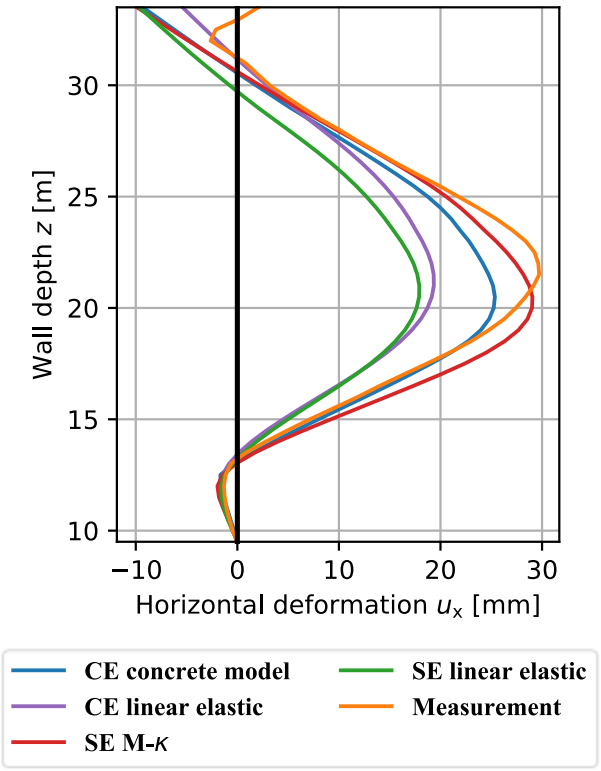

Figure 5. Comparison of the calculated horizontal deformations u_x using different material models for the diaphragm wall and the measured deformations u_x plotted over the wall depth z

Furthermore, Figure 6 shows the calculated bending moments up to the bottom of the wall, so that the unreinforced part of the wall is included in the results. It is evident that the numerical simulations using a linear elastic material model for the wall show almost the same bending moment distribution, regardless of whether CE (purple) or SE (green) are used for the wall discretisation. Considering the SE using the M-κ diagram (red) and the CE using the non-linear concrete material model (blue), the calculated maximum and minimum bending moments are smaller compared to the simulations with linear elastic wall modelling. Especially in the area between the second strut (z = +23.5 m NHN) and the jet grout slab (from z = +12.5 m NHN to z = +10.5 m NHN), the bending moments are smaller.

It is also noticeable that the bending moment distribution over depth fluctuates for the simulation using the concrete material model (blue). This is due to the evaluation process using the „*structural forces in volume plates*“ feature, where the results of the stress points are integrated along a cross-section line. Compared to the results from the non-linear material model with the M-κ relation (red), the moment curve is comparable up to the second strut (z = +23.5 m NHN). Below this point, the bending moment distributions start to deviate with smaller values in the field (z = +19 m NHN) as well as in the area of the jet grout slab (from z = +12.5 m NHN to z = +10.5 m NHN). In this respect, further investigations are necessary, as differences between the two non-linear material models (concrete - blue curve and M-κ - red curve) also occur regarding the horizontal wall deformation.

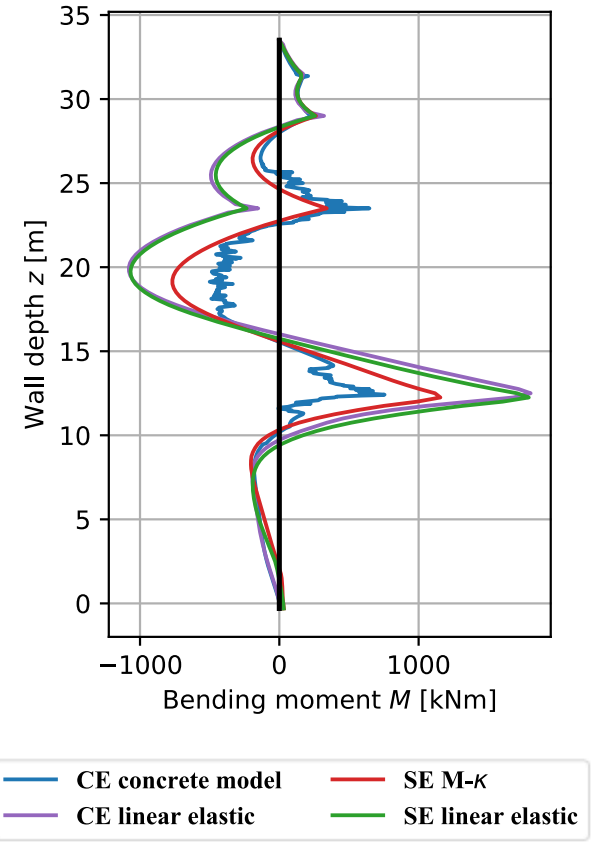

Figure 6. Comparison of the calculated bending moments M using different material models for the diaphragm wall plotted over the wall depth z

Table 3 shows the calculated normal forces at the supports with respect to the different simulation approaches. The normal force from the simulations with the non-linear material models (c and d) at the second strut $N_{Strut,bottom}$ is higher, compared to the results from the simulations with linear-elastic wall behaviour

(a and b). Considering the deformation of the wall (Figure 5), it is clear that the wall deflects more if the non-linear material models are used, which means that the supports receive higher normal forces.

Table 3. Comparison of the calculated normal forces at the supports for the investigated modelling approaches

Normal Forces [kN]	**Modelling approaches**			
	CE - LE (a)	SE – LE (b)	SE – M-κ (c)	CE - Conc. (d)
N_{Anchor}	457.3	431.7	442.6	434.2
$N_{Strut,top}$	2992.1	3226.7	3120.5	3007.1
$N_{Strut,bottom}$	3461.1	3461.8	4620.9	4534.8

5 CONCLUSIONS

This paper investigates an excavation pit located in Berlin that is supported by two struts and one anchor. Based on available measurement data, the stiffness parameters of the soil are initially calibrated by using a Particle Swarm Optimization, so that parameters of the Hardening Soil material model considering the small strain stiffness are applicable. The parameters are optimized until the difference between calculated and measured horizontal deformations in the final state of the excavation is minimized. The results of the inverse parameter identification show that no set of parameters can be found for which the calculated and measured horizontal deformations of the diaphragm wall are in good agreement. The reasons for this may be complex and provide a framework for further research.

In this paper, a numerical forensic investigation is carried out to investigate the influence of the material models used to discretise the diaphragm wall material. For this purpose, the parameters obtained from of the PSO (best fit) are used as the basis for a comparison considering four different modelling variants for the diaphragm wall: continuum elements as well as a structural element considering linear-elastic material behaviour, an elastoplastic structural element with a user-defined M-κ diagram and continuum elements considering an elastoplastic concrete model.

The results show that larger wall deformations are calculated by means of elastoplastic diaphragm wall modelling compared to “classical” linear-elastic simulations. Therefore, it can be concluded that in the investigated case plastic wall deformations occurred during the excavation process. Regarding the bending moments, the higher wall deformation leads to larger normal forces at the bottom strut and smaller bending moments in the field near the base of the excavation pit compared to simulations considering linear-elastic wall modelling.

In conclusion, the present paper highlights that the use of elastoplastic material modelling of concrete walls for deep excavation pits may be necessary for realistic prediction of wall deflections as well as bending moment distribution. Regarding the available elastoplastic material models, both models are well suited for realistic evaluation of the above mentioned results although a M-κ relationship with structural elements has advantages regarding the evaluation of bending moments.

Regarding the concrete material model, it can be stated that this model enables a realistic modelling of the wall deformation behaviour and can lead to a more realistic simulation of the detailed plastification process, but further research and development is necessary regarding the evaluation of internal forces.

6 ACKNOWLEDGEMENTS

The authors want to thank Dr.-Ing. Arne Kindler from Stump-Franki Spezialtiefbau GmbH for providing the required measurement data and documents of the investigated excavation pit as well as for the fruitful discussions.

7 REFERENCES

Schweiger, H.F., Pouya, S., Henke, S., Borchert, K.-M. 2014. Numerical modelling of ground improvement techniques considering tension softening. *Proceedings of the 8th International Symposium on Geotechnical Aspects of Underground Construction in Soft Ground* (Eds: Park, S.-W., Kim, B. & Ban, H.), 209-214. Korean Geotechnical Society, Seoul, South Korea.

Schädlich, B., Schweiger, H.F. 2014. A new constitutive model for shotcrete. *Numerical methods in geotechnical engineering* (Eds: Hicks, M.A., Brinkgreve, R.B.J. & Rohe, A.), 103-108. Taylor & Francis Group, London.

Kennedy, J., Eberhart, R. 1995. Particle swarm optimization. *Proceedings of IEEE International Conference on Neural Networks, Volume IV,* 1942-1945, Perth, Australia, IEEE Service Center, Piscataway, NY.

Schanz, T., Vermeer, P.A., Bonnier, P.G. 1999. Formulation and verification of the Hardening-Soil Model. *Beyond 2000 in Computational Geotechnics* (Ed: Brinkgreve, R.B.J.), 281-290. Balkema, Rotterdam.

Benz, T. 2007. *Small Strain stiffness of soils and its numerical consequences*, Institut für Geotechnik, Stuttgart.

Hajihassani, M., Jahed Armaghani, D., Kalatehjari, R. 2018. Applications of Particle Swarm Optimization in Geotechnical Engineering: A Comprehensive Review, *Geotechnical and Geological Engineering* **36**, 705-722.

Meier, J., Rudolph, S., Schanz, T. 2009. Effective algorithm for parameter back calculation - Geotechnical applications, *Bautechnik* **86.S1**, 86-97.

Levasseur, S., Malécot, Y., Boulon, M., Flavigny, E. 2008. Soil parameter identification using a genetic algorithm, *International Journal for Numerical and Analytical Methods in Geomechanics* **32.2**, 189-213.

op de Kelder, M. 2015. 2D FEM analysis compared with the in-situ deformation measurements: A small study on the performance of the HS and HSsmall model in a design, *Plaxis Bulletin* **38**, 10–17.